Dalton Transactions

Accepted Manuscript

ROYAL SOCIETY OF CHEMISTRY

www.rsc.org/dalton

Journal Name

RSCPublishing

ARTICLE

Temperature-Dependent Upconversion Luminescence and Dynamics of $NaYF_4:Yb^{3+}/Er^{3+}$ Nanocrystals: Influence of Particle Size and Crystalline Phase

Cite this: DOI: 10.1039/xoxxoooooox

Received ooth January 2012,
Accepted ooth January 2012

DOI: 10.1039/xoxxoooooox

www.rsc.org/

Wei Yu, Wen Xu, Hongwei Song* and Shuang Zhang*

Oleic acid capped $NaYF_4:Yb^{3+}/Er^{3+}$ upconversion nanocrystals (UCNCs) with different sizes and crystalline phases were prepared, and their temperature-dependent upconversion luminescence (UCL) and dynamics were studied. It is interesting to observe that the temperature-dependent behavior of UCL for β-phase (25-nm, 45-nm and bulk) and α-phase (<10 nm) UCNCs is quite different. The UCL intensity of Er^{3+} ions of the β-phase $NaYF_4$ demonstrates a maximum around 100 K, while the intensity of the α-phase one quenches monotonously with the elevated temperature (10-400 K). The intensity ratio of $^2H_{11/2}$-$^4I_{15/2}$ to $^4S_{3/2}$-$^4I_{15/2}$, R_{HS}, increases solely with temperature for β-phase $NaYF_4$, while for the α-phase sample, it demonstrates a complex and indecisive variation as a function of temperature. In the β-phase samples, rising processes were observed in the dynamics of Er^{3+} ions, while in the α-phase sample, no rising process was observed and the decay processes of Er^{3+} ions were bi-exponential. The essential of these different temperature-dependent UCL properties was explained carefully.

1. Introduction

Upconversion (UC) phosphors, which can convert a low frequency excitation photon into a high frequency emission photon through two-photon or multi-photon processes, have attracted great interests in recent several decades owing to their unique photoluminescent features and a large number of application potentials, such as background lighting source, solid state lasers, infrared detection, solar cell conversion and etc.[1-6] In particular, some rare earth (RE) doped fluoride UCNCs, are attracting extensive current interests because of their relatively high UC efficiency and significant application potential in the field of in vivo imaging, infrared (IR) photo-dynamical therapy, bio-labels and bio-sensors.[7-9] Among various fluoride UC phosphors, the microsized polycrystalline powder of β-phase $NaYF_4$:Yb, Er is considered as one of the most efficient under the excitation of a 980-nm laser diode, however, it's UC efficiency is only 3 %, and that of the corresponding nanosized phosphors(~10nm) is only one of tenth of the microsized.[10,11] Therefore, it is key important to further improve the efficiency of the fluoride UC phosphors and to search for novel efficient UC phosphors.

It is known that the UCL strongly depends on dopant concentrations, excitation power, crystallite phases and particle sizes, and thermal conditions.[12-15] Actually, there are two types of crystallite phases exist in $NaYF_4$ at ambient pressure and temperature: the cubic phase (α-phase) and the hexagonal phase (β-phase). It was reported that the UC intensity of the green emission of β-$NaYF_4$:Yb, Er is 10 times stronger than that of α-$NaYF_4$:Yb, Er and the overall (green plus red) emission of the former is 4.4 times higher than that of the latter and the.[16-18] Generally, with the decrease of particle size, the UC strength was suppressed due to the improved surface adsorption of large phonon bonds, such as water and the unexpected crystallinity of smaller nanoparticles (NPs), and, the ratio of the green to the red was also considerably modulated.[19,20] Despite a number of studies related to $NaYF_4$:Yb, Er UCNCs have been performed, yet, some significant problems have not been completely

understood. For instance, essentially, how the change of crystalline phase as well as particle size influence the UCL of the phosphors, including radiative transition, noradiative relaxation and ET processes.

The studies on temperature-dependent UCL and dynamics of $NaYF_4$:Yb, Er UCNCs with different particle sizes and crystalline phases is significant of understanding these questions. Temperature has two effects on the UCL of nano-materials. On the one hand, it can generate heat radiation and stimulated luminescence, on the other hand, it promotes the nonradiative transitions and the quenching.[20-22] The study of their variable temperature spectra will help to further understand UC mechanisms and the use of the materials for potential thermal sensing and biosensor applications.[21,23] It was reported[24] that the luminescent intensities of Er^{3+} and Yb^{3+} codoped Y_2O_3 nanocrystals decreased with the increasing temperature from 10 K to 300 K. This effect was explained by the enhancement of nonradiative multiphonon relaxation rates, which reduces the radiative transition probability at high temperatures. Van Der Zielet al.[25] found that the intensities of YF_3 increased and then decreased with the temperature raising up to room temperature. The depopulation of the higher sublevels of the $^4I_{11/2}$ at lower temperatures and multiphonon deexcitation at higher temperatures were proposed as dominant factors that govern the temperature-dependent behavior. Shan et al.[26] reported UCL of $NaYF_4$:Yb^{3+},Er^{3+} UCNCs at various temperatures from 300 K to 450 K and observed similar phenomenon. So far, there has no a complete work related to temperature-dependent UCL and dynamics of $NaYF_4$:Yb, Er with different sizes and crystalline phases.

In the present work, we prepared oleic acid (OA) capped $NaYF_4$:Yb^{3+},Er^{3+} NCs with different sizes and phases and investigated their temperature-dependent UCL and dynamics systemically. Some interesting temperature-dependent UCL properties were observed, which depended on both the crystalline phase and particle size of $NaYF_4$:Yb^{3+},Er^{3+} UCNCs.

2. Experimental Section

2.1. Materials.

All of the chemicals used were of analytical grade and were used without further purification. NaOH, NH_4F, Methanol, and cyclohexane were purchased from Sinopharm chemical Reagent Co., Ltd. Octadecene were purchased from Sigma(America). OA (>90%) was obtained from Alfa Aesar. Rare earth (RE) chlorides ($LnCl_3$, Ln: Y, Yb, Er) (>99.99%) were purchased from Baotou Ruike Functional Materials Co. Ltd.

2.2. Synthesis of $NaYF_4$:Yb, Er UCNCs

The OA capped $NaYF_4$:18%Yb, 2%Er NCs were synthesized following a procedure reported previously[27]. Firstly, YCl_3 (0.2416 g), $YbCl_3$ (0.0697 g) and $ErCl_3$ (0.0077 g) were mixed with 6 ml OA and 15 ml octadecene(ODE) and heated to 160 ◦C to form a homogeneous solution, and then cooled down to room temperature. Then, 10 ml methanol solution containing NaOH (0.1 g) and NH_4F (0.148 g) were slowly added into the solution with magnetic stirring, then the solution was stirred continuously for 30 min. Subsequently, the solution was heated to 120 ◦C to form a pellucid solution and remove residual water and oxygen, then heated to 280, 300, or 320 ◦C and maintained for 1 h under nitrogen atmosphere to prepare NCs with different sizes. After the solution was cooled down naturally, NCs were precipitated from the solution with ethanol and washed with cyclohexane for three times. The bulk material was obtained by annealing the 320 ◦C sample at 600 ◦C for 3 hours.

2.3. Characterization

The size and morphology of as-prepared UCNCs were recorded on a Hitachi H-8100IV transmission electron microscope (TEM) under an acceleration voltage of 200 kV. The as-prepared samples were dispersed in cyclohexane and dripped onto a copper grid for the TEM tests. The crystalline structure and purity of the as-prepared samples were characterized by X-ray power diffraction (XRD) with a Rigaku D/max 2550 X-ray diffractometer, using a monochromatized Cu target radiation resource (λ = 1.54 Å). The UCL spectra were measured by Andor Shamrock SR-750 fluorescence spectrometer. A CCD detector combined with a monochromator was used for signal collection from 300 nm to 850 nm. A continuous 980 nm diode laser was used to pump the samples for the measurement of steady-state emission spectra. In the measurement of UC dynamics, a tunable Nd:YAG laser pumped OPO laser was used as excitation source. It was with a pulse duration of 10 ns, repetition frequency of 10 Hz and line width of 4-7 cm^{-1} and was fixed at 980 nm. All were tested under vacuum, and the temperature was changed from 10 K to 400 K.

3 Results and Discussion

3.1 Structure and Morphology of the $NaYF_4$:Yb, Er UCNCs

The transmission electron microscopy (TEM) images of as-prepared $NaYF_4$ prepared at different temperatures are shown in Figure 1(a-c), scanning electron microscope (SEM) image in Figure 1(d). A histrogram of the particle size distribution was obtained by direct observation on TEM bright field images, as shown in Figure 1 (e-g). It can be seen that when the reaction temperature was at 280 °C, small $NaYF_4$ UPNCs were formed and they showed a rather wide size distribution. The mean particle size was determined to be 6.5±6.1 nm. From the high-resolution patterns, a fringe with lattice distance of 0.3 nm was observed, corresponding to the (111) face of cubic $NaYF_4$, implying the formation of crystalline phase, however, it is also clear that some regions were with amorphous phase. As the temperature increased further, the average sizes of $NaYF_4$ UCNCs increased and became homogeneous, which showed 25±1.5 nm when prepared at 300 °C, 45±1.9 nm at 320 °C, respectively. For the annealed bulk sample (see Figure 1 (d)), the shape of particles is irregular due to the accumulation of small NPs, and the size of the particles ranges of several

hundreds nanometers to several micrometers. Figure 1h show the XRD patterns of the as-prepared $NaYF_4$ UCNCs fabricated at different temperatures in comparison to the standard cards of α-$NaYF_4$ and β-$NaYF_4$. It can be distinguished that the samples prepared at 280 °C demonstrate cubic in phase (JCPDS: 077-2042). As the reaction temperature increases to 300 °C, $NaYF_4$ has transformed into β-phase. At higher temperature, the pure hexagonal phase also appears (JCPDS standard card no. 28-1192).

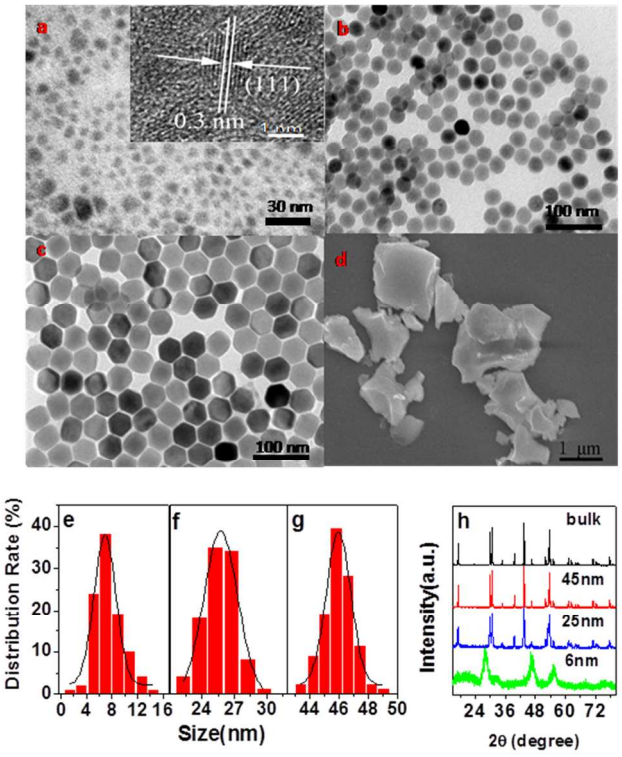

Figure 1 TEM images(a-c), SEM image(d), size distribution(e-g) and XRD(h) patterns of $NaYF_4$:Yb^{3+}, Er^{3+} nanocrystals at different reaction temperatures of 280 ◦C (a, e cubic phase, JCPDS: 077-2042), 300 ◦C (b, f hexagonal phase), and 320 ◦C (c, g hexagonal phase) and bulk (d, hexagonal phase).

3.2 Power-dependence of $NaYF_4$:Yb,Er UCNCs

The normalized UCL spectra of $NaYF_4$:Yb, Er UCNCs with different sizes under the excitation of a 980-nm laser diode are shown in Figure 2a. In all the emission spectra of $NaYF_4$:Yb, Er UCNCs, the blue $^2H_{9/2}$-$^4I_{15/2}$, green $^4S_{3/2}$, $^2H_{11/2}$-$^4I_{15/2}$ and red $^4F_{9/2}$-$^4I_{15/2}$ transitions can be clearly identified. The green emissions of $^4S_{3/2}$, $^2H_{11/2}$-$^4I_{15/2}$ are dominant for all the samples. It can be seen that the intensity ratio of the red to green, slightly increases with the decreasing particle size. It should be noted that the overall emission intensity of the samples increases considerably with the increasing particle size, as reported by the previous literatures. Previously, we systemically studied the size-dependent UCL behavior of $NaLuF_4$:Yb, Er with different phases, α-phase and β-phase, and observed that they demonstrated opposite results, in the β-phase $NaYF_4$ the intensity ratio of the red to green slightly increases with the decreasing particle size, on the contrary, in the α-phase sample, the intensity ratio of the red to green decreases remarkably with the decreasing particle size. The difference of size-dependence UCL between α-phase and β-phase samples was attributed to the contribution of cross relaxation processes.[30] In the α-phase samples, the cross relaxation process happened easily due to the random distribution of rare earth ions, while in the β-phase samples, the cross relaxation process happened hardly due to the strict distribution of rare earth ions.[30]

Figure 2b shows the schematic of the UC excitation pathways and the emission processes for the $NaYF_4$:Er^{3+},Yb^{3+} under 980-nm excitation.[19] Firstly, Er^{3+} ions on $^4I_{15/2}$ are excited to $^4I_{11/2}$ by the ground state absorption (GSA) and/or energy transfer (ET) of Yb^{3+}-Er^{3+}. Then the same laser pumps the excited-state electrons from the $^4I_{11/2}$ to the $^2H_{11/2}$ levels via excited-state absorption (ESA) or the second-step ET of Yb^{3+}-Er^{3+}, the electrons relax to $^4S_{3/2}$, $^2H_{11/2}$, generating green $^4S_{3/2}$, $^2H_{11/2}$-$^4I_{15/2}$ transitions. The populating pathway of the red $^4F_{9/2}$ level is as follows: after populating $^4I_{11/2}$ level, the electrons further relax to $^4I_{13/2}$, then are excited into $^4F_{9/2}$, generating $^4F_{9/2}$-$^4I_{15/2}$ transitions. Besides, the nonradiative relaxation from the green $^4S_{3/2}$, $^2H_{11/2}$ level to $^4F_{9/2}$ is another pathway for the population of the red. The populating of the blue is a three-photon process: Some of the electrons on the red $^4F_{9/2}$ are further excited into $^2H_{9/2}$ through the third-step ET of Yb^{3+} to Er^{3+}, and generating blue $^2H_{9/2}$-$^4I_{15/2}$ transitions. Generally speaking, as the particle size decreases, due to the increase of the ratio of surface to volume, a number of surface defects with available large vibrational modes such as CO_3^{2-} and OH^- are involved. Large vibrational modes results in the increase of nonradiative relaxation channels, $^4I_{11/2}$-$^4I_{13/2}$ and $^4S_{3/2}$, $^2H_{11/2}$-$^4F_{9/2}$, leading to the relative increase of the red transitions. It should be also noted that as the doping concentration is high enough, cross relaxation of $^4F_{7/2}$+$^4I_{11/2}$-$^4F_{9/2}$+$^4F_{9/2}$ also happens largely, leading to the relative increase of the red emissions.

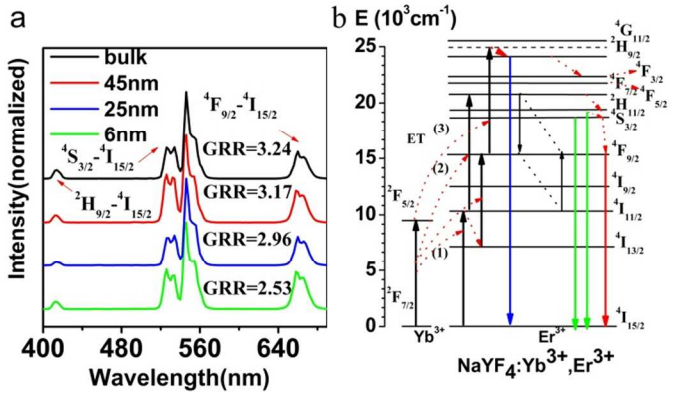

Figure 2 (a) The UCL spectra of $NaYF_4$:Yb^{3+},Er^{3+} with different sizes excited by a 980-nm laser diode of 1.8 W/mm^2. (b) The achematic of the luminescence processes of $NaYF_4$:Yb^{3+},Er^{3+} under the excitation of 980 nm

light. The solid lines present radiative transitions and the dash lines are nonradiative ones.

To further reveal the UC mechanism, the blue ($^2H_{9/2}$-$^4I_{15/2}$), green ($^2H_{11/2}$/$^4S_{3/2}$-$^4I_{15/2}$) and red ($^4F_{9/2}$-$^4I_{15/2}$) emissions were measured as a function of excitation power, as shown in Figure 3. Following the UC mechanism, the visible emission intensity is proportional to a certain power (n) of the infrared excitation intensity. For the blue emission, the values of n were determined to be 1.43, 2.19, 1.29 and 1.12. For the green emission, the values of n were determined to be 1.38, 1.62, 1.34, and 1.92, respectively. For the red emission the values of n were determined to be 1.40, 1.97, 1.49 and 1.04. As is well

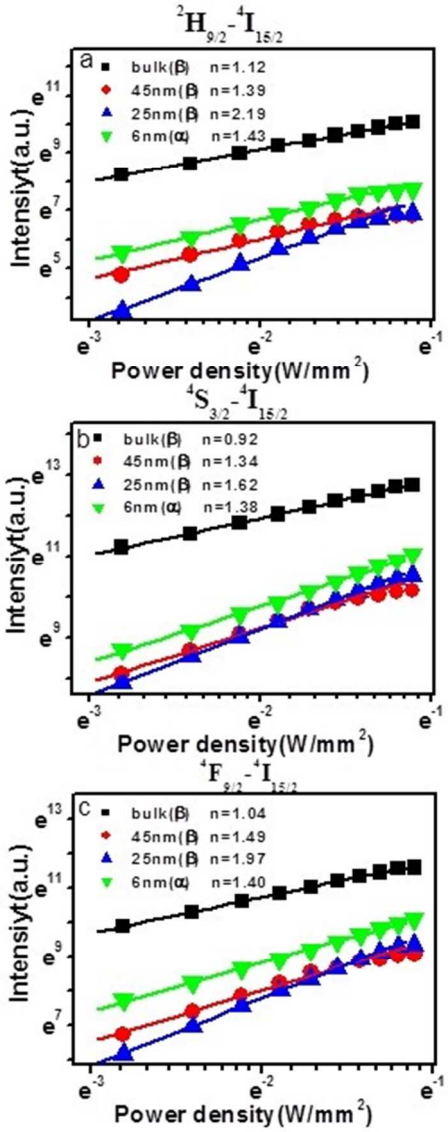

Figure 3 Plot (ln-ln) of emission intensity versus excitation power in different size particles. (a) the blue emission, (b) the green emissionand, (c) the red emission.

known, for any upconversion mechanism, the value of n presents the number of IR photons absorbed per visible photon emitted. For the two-photon processes (the red, green emissions), n should equal or be close to 2 and for the three photon processes (the blue), n should be close to 3. However, in our experiment, the values of n were much smaller than the photon number for the transitions. This was mainly attributed to the competition between linear decay and UC processes for the depletion of the intermediate excited states, which was theoretically described by Pollnauet al.[22] It can be deduced that when the particle size decreased from bulk to 25 nm, the value of n increased gradually, which was attributed to the suppression of saturation effect. As the particle size decreased, the linear decay process would increase due to the increase of nonradiative relaxation processes. Oppositely, when the particle size decreased from 25 nm to several nanometer, the value of n decreased, which could be attributed to highly improved local thermal effect. For the 6-nm UCNCs, nonradiative transition process will increase significantly due to its worse crystallinity and improved surface adsorption. The local thermal effect will induce the temperature of the sample at the irradiated site increases with the excitation power. Slight thermal quenching will lead the value of n to decrease, while strong thermal quenching will even lead the UCL intensity to decrease with the excitation power.[28]

3.3 Temperature-dependent UCL spectra of $NaYF_4$:Yb, Er NCs

The temperature-dependent UCL of $NaYF_4$:Yb^{3+},Er^{3+} NCs with different sizes were compared under 980-nm excitation, as shown in Figure 4. It is interesting to observe that for the 6-nm α-phase sample, the intensity of UCL decreases solely with the increase of temperature for all the red, green and blue transitions, which can be attributed to significant thermal quenching of UCL due to its worse crystallinity and surface adsorption of water. For the other β-phase UCNCs (25 nm, 45 nm and bulk), totally to say, the UCL intensity of Er^{3+} ions first increases with elevated temperature, and it demonstrates an optimum at a certain temperature, and then decreases with further increase of temperature, for all the transitions. For the bulk sample the optimum appears around 100 K, and for the 25-nm and 45-nm samples, the optimum appears around 150 K. Suyver[29] et al. pointed out that there is an energy gap between the two lowest crystal-field components $^2F_{5/2}|0>$ and $^2F_{5/2}|1>$ of the Yb^{3+} ions and the ET from $^2F_{5/2}|1>$ to the lowest energy crystal-field component $^4I_{11/2}$ state of the Er^{3+} ions is very efficient. On one hand, with the increase of temperature, the relative population on $^2F_{5/2}|1>$ of the Yb^{3+} ions will increase, leading to the increase of the excitation of Yb^{3+}, as a consequence, the ET from Yb^{3+} to Er^{3+} will be more efficient, and the UCL intensity increases with the increase of temperature. On the other hand, the nonradiative relaxation processes will increase with the increase of temperature, leading to the quenching of UCL. These two competition processes lead the appearance of an optimum of UCL intensity at a certain temperature.

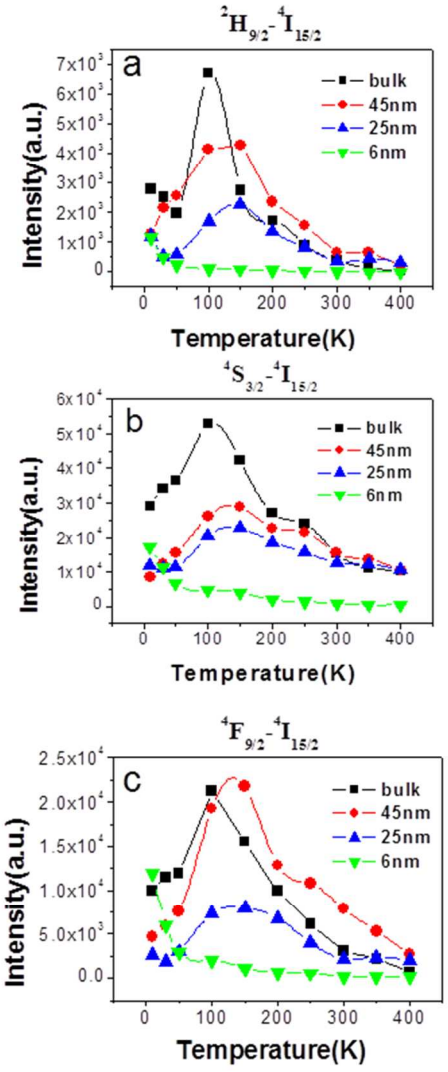

Figure 4 Difference in up-conversion emission intensity of $NaYF_4$:Yb^{3+},Er^{3+} nanoparticles and bulk when taken as dry powder and excited at under the 980 nm LD excitation with the same power density (2.9 W/mm^2) at verified temperature from 10 K to 400 K in vacuum. Blue light(a), green light(b) and red light(c).

Figure 5(a) shows the temperature-dependent UCL spectra of the 6-nm α-phase. For the 6-nm sample, the UCL of $^2H_{11/2}$, $^4S_{3/2}$-$^4I_{15/2}$ and $^4F_{9/2}$ at 10 K is broader bands and the Stark splitting of the emission lines for different transitions is not obvious. This suggests that the local environments surrounding the Er^{3+} luminescent centers are very disordered and the inhomogeneous broadening of the emission lines is quite great. In the other words, the luminescent centers of Er^{3+} for the worse-crystalline $NaYF_4$ contribute dominantly to the UCL at low temperature (10K-50K). Above 100 K, the broader emission bands nearly disappear and the emission lines with distinct Stark splitting can be clearly identified. The above result indicates that the luminescent centers surrounding the disordered local environments have completely quenched above 100 K due to possible ET from the centers to the defect states.

It should be noted that previously, we studied the frequency-selective excitation spectra of Eu^{3+} ions in some oxide compounds NCs such as Y_2O_3, YVO_4 and indentified different symmetry sites, inner sites and surface sites and observed that the emissions of the centers locating on the surface sites became broader, and the luminescent lifetime of the centers became shorter.[30,31] From Figure 5 (a) it can be also seen that the overall intensity ratio of the red emission to the green emission($R_{r/g}$), and the intensity ratio (R_{HS}) of $^2H_{11/2}$-$^4I_{15/2}$ to $^4S_{3/2}$-$^4I_{15/2}$ also varies significantly with temperature. For instance, it is surprise to observe that R_{HS} as well as $R_{r/g}$ first decreases with the elevated temperature ranging of 10-100 K, and it then increases with the elevated temperature in the range of 150-300 K.

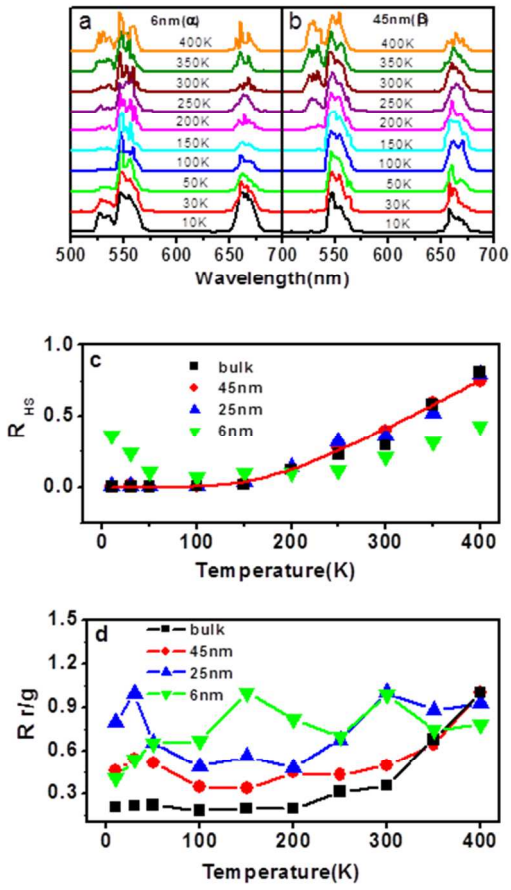

Figure 5 The UCL spectra of $NaYF_4$:Yb^{3+},Er^{3+} nanoparticles of 6 nm(a) and 45 nm(b) when excited at 980 nm at verified temperature from 10 K to 400 K; The intensity ratio of $^2H_{11/2}$-$^4I_{15/2}$ to $^4S_{3/2}$-$^4I_{15/2}$(c).The intensity ratio of red to green(d).

For comparison, the temperature-dependent UCL spectra of the 45-nm β-phase $NaYF_4$ sample are drawn as Figure 5 (b). It can be seen that the 45-nm and the 6-nm samples demonstrate different temperature-dependent UCL behavior. The obvious differences can be concluded as: (1) The stark-splitting of the emission lines for Er^{3+} ions can be distinguished at any

temperature. (2) R_{HS} increases solely with the elevated temperature. As the temperature is below 100K, the transition of $^2H_{11/2}$-$^4I_{15/2}$ can not be indentified due to less electron population of $^2H_{11/2}$. It should be highlighted that for the other samples, (25-nm, bulk), the temperature-dependent behavior of the UCL is similar to that of the 45-nm sample. In order to better understand the temperature-dependent behavior in different samples, R_{HS} and $R_{r/g}$ as a function of temperature in different samples are drawn as Figure 5(c) and 5(d), respectively. As is well known, the intensity ratio R_{HS} of $^2H_{11/2}$-$^4I_{15/2}$ to $^4S_{3/2}$-$^4I_{15/2}$ is sensitive to temperature, and is a critical parameter to mark the temperature change in UCL processes. In Figure 5(c), R_{HS} for the β-phase (25, 45 nm and bulk) $NaYF_4$ UCNCs increases solely with elevated temperature. The population distribution on $^2H_{11/2}$ and $^4S_{3/2}$ should be dominated by Boltzmann's thermal distribution and elevated temperature leads to rapid population of $^4S_{3/2}$-$^2H_{11/2}$. The population ratio of $^2H_{11/2}$-$^4I_{15/2}$ to $^4S_{3/2}$-$^4I_{15/2}$ can be written as,

$$R_{HS} = \alpha e^{-\Delta E/KT} \quad (1)$$

where α is a constant, ΔE is the energy difference between the two levels ($^2H_{11/2}$ and $^4S_{3/2}$), K is Boltzmann's constant, and T is the absolute temperature. The experimental data of the β-phase samples can be fitted by Eq.(1) very well. The 6-nm α-phase $NaYF_4$ sample differs from others, in which the R_{HS} decreases with the increasing temperature and reach a maximum around 100 K. Until now, this behavior has not been completely understood. Previously, Liu GK and his co-workers studied the temperature-dependence of photoluminescence of Er^{3+} ions in Y_2O_3 nantubes and also observed indecisive phenomenon. They observed that even at low temperature (~10K), the population of $^2H_{11/2}$ could not be neglected and the photoluminescence of $^2H_{11/2}$ -$^4I_{15/2}$ could be observed, unlike the microsized powders and they attributed it to the contribution of special electron-photon coupling modes for one-dimensional NPs.[32] In the present case, we suggest that the indecisive temperature-dependence of R_{HS} for the 6-nm sample is related to the imperfect crystallinity of it. In the disordered system of local environment, the nonradiative transition rate of $^2H_{11/2}$-$^4S_{3/2}$ might be very large and might be comparable to the radiative transition rate of $^2H_{11/2}$-$^4I_{15/2}$ and even the thermal activation rate of $^4S_{3/2}$-$^2H_{11/2}$. On the case, R_{HS} can not be simply described by the Eq.(1), but should be described by a modified model.[35] It should be also pointed out that the indecisive relationship between R_{HS} and temperature might be also related to the local thermal effect induced by the laser irradiation.

The intensity ratios $R_{r/g}$ as a function of temperature were also obtained, as shown in Figure 5(d). It can be observed that for the bulk sample, $R_{r/g}$ increases solely with the elevated temperature, which can be attributed to the increase of nonradiative relaxation rates of $^4S_{3/2}$-$^4F_{9/2}$, $^4I_{11/2}$-$^4I_{13/2}$. For the other samples, the variation tendency is similar above 100 K, however, the variation degree is not as large as the bulk sample. And, the variation below 100 K is more complex.

3.4 Temperature-dependent UCL Dynamics

In order to deeply understand the UCL behavior in $NaYF_4$:Yb^{3+}, Er^{3+} UCNCs with different sizes and phases, the temperature-dependent dynamical processes of the excited states ($^4F_{13/2}$, $^4S_{3/2}$, $^4F_{9/2}$) for Er^{3+} ions were measured and compared under the excitation of a 980-nm pulsed laser. Figure 6 shows the typical dynamical processes of 6 nm (α-phase) and 45 nm (β-phase) $NaYF_4$:Yb^{3+}, Er^{3+} at different temperatures. It can be seen that in the 6-nm α-phase sample no rising process was observed for all the $^2H_{9/2}$-$^4I_{15/2}$, $^4S_{3/2}$-$^4I_{15/2}$ and $^4F_{9/2}$-$^4I_{15/2}$ transitions (see Figure 6 a-c). An immediate decay of the emission intensity after the excitation pulse (without a rise) points toward ground state absorption followed by excited state absorption (GSA/ESA).[33]

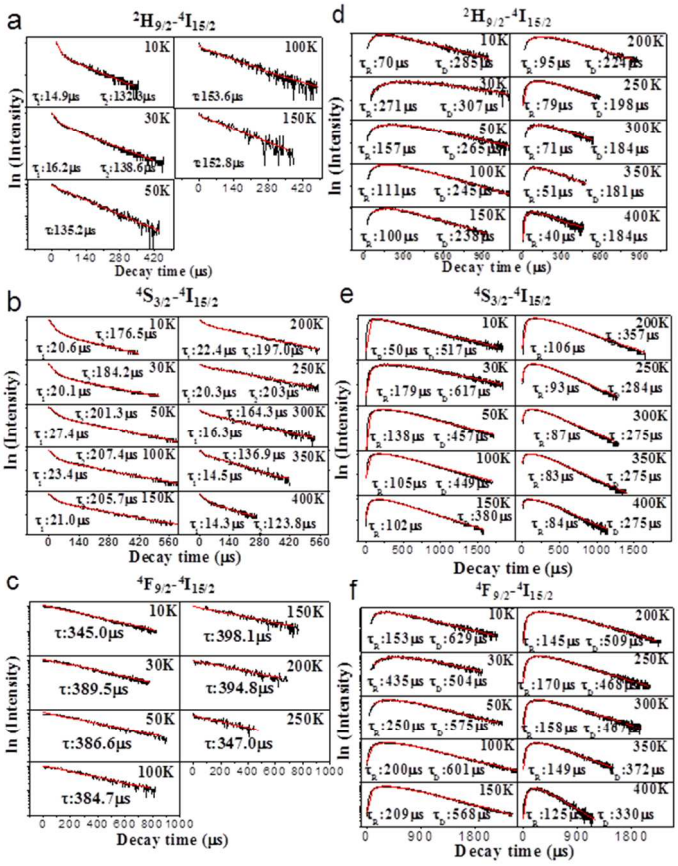

Figure 6 The UCL decay time of the transitions at 416 nm, 544 nm and 656 nm of Er^{3+} ions in 6 nm α-$NaYF_4$(a), (b) and (c); 45nm β-$NaYF_4$(d), (e) and (f) samples with different temperature.

This result suggests that as the particle size is small enough, the ET from Yb^{3+} to Er^{3+} is insufficient. There are several possible factors leading to this point. First of all, as the particle size decreases to several nanometers, the ET efficiency will be suppressed due to the boundary effect of nanoparticles.[34] Second, in the α-phase UCNCs prepared at relatively low temperature, a number of defect states should be involved,

which can be judged from imperfect crystallinity of the sample. And more, a number of large phonon bonds such as OH^- groups would be involved unavoidably on the surface of the nanoparticles.[32] These two facts will result in the improvement of nonradiative ET processes from Yb^{3+} ions to defect states and/or OH^- groups, which compete with the ET processes from Yb^{3+} to Er^{3+}. From Figure 6(a-c) it can be also seen that for the $^2H_{9/2}$-$^4I_{15/2}$ and $^4S_{3/2}$-$^4I_{15/2}$ transitions, the decays of the emission intensities are all bi-exponential, which depend strongly on temperature and can be written as,[36]

$$I(t)=I_1exp(-t/\tau_1)+I_2exp(-t/\tau_2), \quad (2)$$

Where τ_1 and τ_2 represent the shorter and longer lifetime constants, respectively, and I_1, I_2 are the original contribution for the shorter and longer decay times. The shorter time constants range of several ten microseconds, while the longer time constants range of several hundred microseconds. From the temperature-dependent dynamics it can be seen that for the $^2H_{9/2}$-$^4I_{15/2}$ transition, the contribution of the shorter decay process decreases quickly with the increasing temperature, and when the temperature is above 30 K, the shorter decay process nearly disappears. For the $^4S_{3/2}$-$^4I_{15/2}$ transition, the relative contribution of the shorter decay process slowly decreases with the elevated temperature. It is suggested that the appearance of bi-exponential decay processes comes from the emissions of Er^{3+} ions at different local environments, the shorter process corresponds to the emissions of Er^{3+} ions with disordered local environment or on the surface of nanoparticles, while the longer process corresponds to the emissions of Er^{3+} ions at relatively neat crystalline local environment. It should be noted that in some of our previous works, we studied the site symmetry of some oxide compounds, such as Y_2O_3:Eu^{3+} and YVO_4:Eu^{3+} nanowires and nanoparticles by laser-selective excitation and observed that as the particle size decreases to several nanometers, the emissions of Eu^{3+} ions origanating from surface sites occur, which are with relatively broad lines and short lifetimes.[37,38]

The UCL of Er^{3+} ions with different local environments demonstrate different temperature-dependent behavior. The emissions of Er^{3+} ions with disordered local environments demonstrate quick temperature-quenching, while Er^{3+} ions with neat crystalline local environments yield slow temperature-quenching. This is well in accordance with the temperature-dependence of emission spectra.

The temporal evolution of β-phase $NaYF_4$:Yb^{3+}, E^{3+} (45 nm) as a function of time can be fitted to a Vial's type equation, for all the $^2H_{9/2}$-$^4I_{15/2}$, $^4S_{3/2}$-$^4I_{15/2}$ and $^4F_{9/2}$-$^4I_{15/2}$ transitions:

$$I(t)=I_1exp(-t/\tau_D)-I_2exp(-t/\tau_R), \quad (3)$$

where τ_D and τ_R represent the decay and the rise of the emission, respectively. τ_D is essentially the UCL lifetime, which is essentially influenced by the lifetime of the emitting level and the lifetime of the levels feeding the excited states through the energy transfer process. The rise time τ_R is determined *by* the lifetime of the emitting state and the ET rate from Yb^{3+} to Er^{3+}.[37,39] From the best fitting functions it can be seen that the rising time constant first increases with the increase of temperature when the temperature varies from 10K to 30K, and it then decreases with the further increase of temperature. It should be noted that for the 25-nm and bulk samples, their luminescent dynamics are similar to those of the 45-nm samples, and their- temperature-dependent dynamics are drawn as Figure S1 and Figure S2, respectively.

In order to better understand the temperature-dependent luminescent dynamics, the rising and decay time constants as a function of temperature for different samples are drawn as Figure 7. It can be seen that the rising time constants for the 25-nm, 45-nm and the bulk samples demonstrate similar variation tendency. Generally to say, in the 25-nm, 45-nm and the bulk

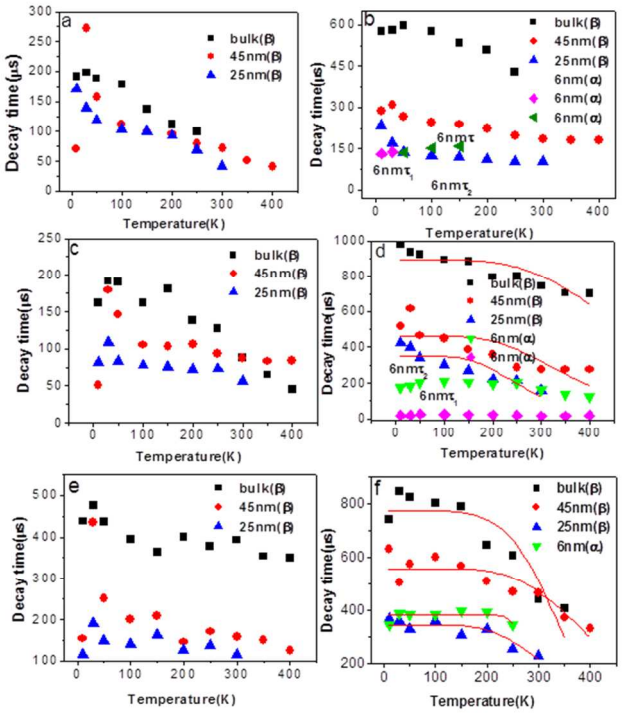

Figure 7 Decay time constant versus temperature of $NaYF_4$:Yb^{3+},Er^{3+} NCs with different size. The rising time of $^2H_{9/2}$-$^4I_{15/2}$(a); decay time of $^2H_{9/2}$-$4I_{15/2}$(b); rising time of $^4S_{3/2}$-$^4I_{15/2}$(c); decay time of $^4S_{3/2}$-$^4I_{15/2}$(d); rising time of $^4F_{9/2}$-$^4I_{15/2}$(e); decay time of $^4F_{9/2}$-$^4I_{15/2}$(f) transition of Er^{3+} ions with different sizes.

samples, for all the transitions the rising time constants first rapidly increase with the increase of temperature from 10 K to 30 K, and then gradually decrease with the increase of temperature above 30 K due to the increase of nonradiative relaxation rates for different emission levels (see Figure (a), (c), (e)). From Figure 7 (b), (d) and (f), it can be seen that for most of cases, the decay time constants decrease with the increase of temperature. As is well known, the decay time constant is reverse of the sum of the radiative and nonradiative transition rates if the cross relaxation processes. The radiative decay rate for an emission level rarely changes with temperature, while the nonradiative decay rate varies significantly with temperature, thus the luminescent lifetime τ for any level can be roughly expressed as,

$$\tau = \frac{1}{W + W(0)[1-\exp(-\hbar\omega / kT)]^{-\Delta E/\hbar\omega}} \quad (4)$$

where W represents the radiative transition rate for the emission levels, $W(0)$ represents the nonradiative transition rate from the emission level to the nearest down level at 0 K, $\hbar\omega$ is the phonon energy for multi-phonon relaxation process and ΔE is the energy gap between the emission level and the nearest down level. The most of experimental data can be well fitted by Eq.(4). By fitting, W and $W(0)$ for different emission levels $^4S_{3/2}$ and $^4F_{9/2}$ were obtained, and the optimum fitting values were listed in Table 1. It can be seen that W increases with the decrease of nanocrystalline particle size. There are two facts affecting the radiative transition rate of RE ions doped NCs, effective refractive index effect and lattice distortion effect.[40] The radiative rate for the electric-dipole transition increases with the increase of refractive index of the phosphor. R. S. Meltzer et al[41] reported that the radiative transition rate of Y_2O_3: Eu NCs is dependent of not only the refractive index itself, but also the surrounding medium, which can be expressed as, $n_{eff} = xn + (1-n)n_{med}$, where x is the filling factor showing what fraction of space is occupied by the nanocrystals and n_{med} is the refractive index of medium. Based on this function, the radiative transition rate for RE ions should decrease in comparison to the corresponding bulk material owing to the effective refractive index effect.[41] However, in some NCs, the unperfected crystallinity could induce the degeneration of lattice symmetry, and thus the radiative transition rate increases with the decrease of particle size.[42] In table 1, it can be also observed that $W(0)$ increases with the decrease of particle size for the $^4S_{3/2}$-$^4I_{15/2}$ transition, however, for the $^4F_{9/2}$-$^4I_{15/2}$ transition, $W(0)$ surprisingly increases with the decrease of particle size, which has not been clearly understood yet.

	Samples	bulk	45nm	25nm	6nm
$^4S_{3/2}$-$^4I_{15/2}$	W/ms^{-1}	1.01	1.25	1.59	5.03
	W(0)/ms^{-1}	0.08	0.75	1.23	
$^4F_{9/2}$-$^4I_{15/2}$	W/ms^{-1}	1.24	1.78	2.4	2.43
	W(0)/ms^{-1}	0.90	0.50	0.47	0.18

Table 1 A list of W and W(0) for different emission levels in $NaYF_4$:Yb^{3+},Er^{3+} samples with different sizes: bulk, 45 nm, 25 nm and 6 nm.

4. Conclusions

In this work, we studied the temperature-dependence of UCL and dynamics of $NaYF_4$:Yb^{3+}, Er^{3+} UCNCs with different particle sizes and crystalline phases and observed some interesting phenomena. First of all, we observed that for the 6-nm α-phase $NaYF_4$:Yb^{3+}, Er^{3+} UCNCs, the overall UCL intensity decreased solely with the increasing temperature, while for the β-phase $NaYF_4$:Yb^{3+}, Er^{3+} UCNCs ranging of several ten to thousands nanometers, the UCL intensity as a function of temperature demonstrated an optimum around 100 K. Second, for the β-phase $NaYF_4$:Yb^{3+}, Er^{3+} UCNCs the intensity ratio of $^2H_{11/2}$-$^4I_{15/2}$ to $^4S_{3/2}$-$^4I_{15/2}$ (R_{HS}) increased solely with temperature and could be well fitted by the Bolzmann's distribution function, while for the α-phase $NaYF_4$:Yb^{3+}, Er^{3+} UCNCs R_{HS} demonstrated a complex and obscure temperature-dependence. Third for the β-phase $NaYF_4$:Yb^{3+}, Er^{3+} UCNCs, the UC dynamics demonstrated a rising process for all the visible UC transitions due to the sufficient ET from Yb^{3+} to Er^{3+}, while for the α-phase $NaYF_4$:Yb^{3+}, Er^{3+} UCNCs, the rising process completely disappeared due to insufficient ET, and the decay processes were bi-exponential due to surface effect. Their physical origins were carefully discussed.

Acknowledgements

This work was supported by National Talent Youth Science Foundation of China (Grant no. 60925018), the National Natural Science Foundation of China (Grant no. 61204015, 51002062, 11174111, 61177042, and 81201738). The China Postdoctoral Science Foundation Funded Project (2012M511337 and 2013T60327).

Notes and references

State Key Laboratory on Integrated Optoelectronics, College of Electronic Science and Engineering, Jilin University, 2699 Qianjin Street, Changchun, 130012, People's Republic of China. E-mail: songhw@jlu.edu.cn

Fax: +86-0431-85155129; Tel: +86-0431-85155129

Electronic Supplementary Information (ESI) available: This text described the addition UCL decay time of the transitions at 416nm 544 nm and 656 nm of Er^{3+} ions in 25 nm α-$NaYF_4$ Figure S1 (a),(b) and (c); bulk β-$NaYF_4$ Figure S2 (a), (b) and (c) samples with different temperature. From the best fitting functions it can be seen that for the 25-nm and bulk samples, their luminescent dynamics are similar to those of the 45-nm samples in our work.

1. L. Sudheendra, V. Ortalan, S. Dey, N. D. Browning and M. Kennedy, Chem. Mater., 2011, **23**, 2987.
2. H. S. Mader, P. Kele, S. M. Saleh and O. S. Wolfbeis, Curr. Opin. Chem., Biol. 2010, **14**, 582.
3. L. Song, X. H. Liu, Z. Zhen, C. Chen and D. J. Zhang, Mater. Chem., 2007, **17**, 4586.
4. Y. J. Ding, X. Teng, H. Zhu, L. L. Wang, W. B. Pei, J. J. Zhu, L. Huang and W. Huang, Nanoscale, 2013, **5**, 11928-11932.
5. F. Wang and X. G. Liu, Chem. Soc. Rev., 2009, **38**, 976-989.
6. X. Teng, Y. H. Zhu, W. Wei, S. C. Wang, J. F. Huang, R. Naccache, W. B. Hu, A. Iing, Y. Tok, Y. Han, Q. C. Zhang, Q. L. Fan, W. Huang, J. A. Capobianco and L. Huang. J. Am. Chem. Soc., 2012, 134, 8340.
7. J. N. Liu, W. B. Bu, L. M. Pan, S. J. Zhang, F. Chen, L. P. Zhou, K. L. Zhao, W. J. Peng and J. L. Shi, Biomaterials, 2012, **33**, 7282.
8. X. J. Kang, Z. Y. Cheng, C. X. Li, D. G. Yang, M. M. Shang, P. A. Ma, G.G. Li, N. Liu and J. Lin, J. Phys. Chem. C, 2011, **115**, 15801.
9. B. T. Chen, B. Dong and J. Wang, Nanoscale, 2013, **5**, 8541.
10. Y. Wei, F. Q. Lu, X. R. Zhang and D. P. Chen, Chem. Mater., 2006, **18**, 5733-5737.
11. H. X. Mai, Y. W. Zhang, L. D. Sun and C. H. Yan, J. Phys. Chem. C, 2007, **111**, 13730.
12. J. W. Zhao, Y. Sun, X. Kong, L. Tian, Y. Wang, L. Tu, J. Zhao and H. Zhang, J. Phys. Chem. B, 2008, **112**, 15666.
13. J. N. Shan and Y. G. Ju, Appl. Phys. Lett., 2007, **91**, 123103.

14. E. S. Zijlstra, T. Janssen, S. R. Lüthi, and H. U. Güdel, Phys. Rev. B, 2000, **61**, 3337.
15. J. F. Suyver, A. Aebischer, S. Garcia-Revilla, P. Gerner and H. U. Güdel, Phys. Rev. B, 2005, **71**, 125123.
16. S. Mishra, G. Ledoux, E. Jeanneau, S. Danielea and M. F. Joubert, Dalton Trans., 2012, **41**, 1490.
17. M. Wang, G. Abbineni, A. Clevenger, C. Mao and S. K. Xu, Nanomedicine: Nanotechnology, Biology and Medicine, 2011, **7**, 710.
18. R. Rossetti, S. Nakahara and L. E. Brus, J. Chem. Phys., 1983, **79**, 1086.
19. S. Schietinger, L. S. Menezes, B. Lauritzen and O. Benson, Nano Lett., 2009, **9**, 2477.
20. Y. S. Chen, W. He, H. H. Wang, X. L. Hao, Y. C. Jiao, J. X. Lu and S. E. Yang, J. Lumin., 2012, **132**, 2404.
21. Y. Q. Lei, H. W. Song, L. M. Yang, L. X. Yu, Z. X. Liu, G. H. Pan, X. Bai and L. B. Fan, J. Chem. Phys., 2005, **123**, 174710.
22. M. Pollnau, D. R. Gamelin, S. R. Lüthi, H. U. Güdel and M. P. Hehlen, Phys. Rev. B, 2000, **61**, 3337.
23. X. Wang, X. G. Kong, Y. Yu, Y. J. Sun and H. J. Zhang, Phys. Chem. C, 2007, **111**, 15119.
24. A. M. Pires, O. A. Serra, S. Heer and H. U. Güdel, J. Appl. Phys., 2005, **98**, 063529.
25. J. P. Van der Ziel, F. W. Ostermayer and L. G. Van Uitert, Phys. Rev. B, 1970, **2**, 4432.
26. J. N. Shan, W. J. Kong, R. Wei, N. Yao and Y. G. Ju, J. Appl. Phys., 2010, **107**, 054901.
27. Z. Q. Li and Y.Zhang, Nanotechnology, 2008, **19**, 345606.
28. Q. L. Dai, H. W. Song, X. G. Ren, S. Z. Lu, G. H. Pan, X. Bai, B. Dong, R. F. Qin, X. S. Qu and H. Zhang, J. Phys. Chem. C, 2008, **112**, 19694.
29. J. F. Suyver, J. Grimm, K. W. Kramer and H. U. Güdel, J. Lumin., 2005, **114**, 53.
30. H. S. Peng, H. W. Song, B. J. Chen, S. Z. Lu and S. H. Huang, Chem. Phys. Lett., 2003, **370**, 485.
31. G. H. Pan, H. W. Song, X. Bai, L. B. Fan, H. Q. Yu, Q. L. Dai, B. Dong, R. F. Qin, S. W. Li, S. Z. Lu, X. G. Ren and H. F. Zhao, J. Phys. Chem. C, 2007, **111**, 12472.
32. G. K. Liu, H. Z. Zhuang and X. Y. Chen, Nano Lett., 2002, **2**, 535.
33. R. Martín-Rodríguez, S. Fischer, A. Ivaturi, B. Froehlich, K.W. Krämer, J. C. Goldschmidt, B. S. Richards and A. Meijerink, Chem. Mater. 2013, **25**, 1912.
34. J. Wang, H. W. Song, W. Xu, B. Dong, S. Xu, B. T. Chen, W. Yu and S. Zhang, Nanoscale, 2012, **5**, 3412.
35. X. Bai, H. W. Song, G. H. Pan, Y. Q. Lei, T. Wang, X. G. Ren, S. Z. Lu, B. Dong, Q. L. Dai and L. B. Fan, J. Phys. Chem. C, 2007, **111**, 13611.
36. S. Xu, W. Xu, B. Dong, X. Bai and H. W. Song, J. Appl. Phys., 2011, **110**, 113113.
37. X. Bai, H. W. Song, L. X. Yu, L. M. Yang, Z. X. Liu, G. H. Pan, S. Z. Lu, X. G. Ren, Y. Q. Lei and L. B. Fan, J. Phys. Chem. B, 2005, **109**, 15236.
38. W. Xu, Y. Wang, X. Bai, B. Dong, Q. Liu, J. S. Chen and H. W. Song, Phys. Chem. C, 2010, **114**, 14018.
39. D. Li, B. Dong, X. Bai, Y. Wang and H. W. Song, J. Phys. Chem. C, 2010, **114**, 8219.
40. J. K. Li, J. G. Li, Z. J. Zhang, X. L. Wu, S. H. Liu, X. D. Li, X. D. Sun and Y. Sakka, Adv. Mater., 2012, **13**, 035007.
41. R. S. Meltzer, S. P. Feofilov and B. Tissue, Phys. Rev. B, 1999, **60**, R14012.
42. H. W. Song, J. Wang, B. Chen, H. Peng and S. Lu, Chem. Phys. Lett., 2003, **376**, 1.